Faraday Discussions

Cite this: *Faraday Discuss.*, 2025, **258**, 307

ROYAL SOCIETY OF CHEMISTRY

PAPER

View Article Online
View Journal | View Issue

Low-cost electrochemical gas sensing of vertical differences in wintertime air composition (CO, NO, NO_2, O_3) in Fairbanks, Alaska†

Tjarda J. Roberts, *[ab] Meeta Cesler-Maloney [c] and William R. Simpson [c]

Received 12th November 2024, Accepted 2nd January 2025
DOI: 10.1039/d4fd00177j

Wintertime Fairbanks, Alaska, experiences episodes of severely poor air quality, when local emissions (*e.g.*, home-heating, vehicular) are enhanced by cold conditions and are trapped by temperature inversions. Monitoring of atmospheric composition, and in particular vertical gradients in composition, is challenging under cold Arctic conditions. This study demonstrates that multiple sets of low-cost electrochemical sensors can provide accurate measurement of CO, NO, NO_2, and O_3 air composition across wide-ranging cold Arctic temperatures (0 °C to −30 °C). The sensors quantify vertical gradients in downtown Fairbanks' atmospheric composition during winter 2021. Low-cost electrochemical sensors (with temperature co-measured) were characterised by cross-comparison to a regulatory air-quality monitoring site. We demonstrate excellent agreement of the electrochemical sensors with the reference monitors (R^2 > 0.86–0.98), with mean absolute errors <5 ppbv (NO, NO_2, O_3) and <50 ppbv (CO) over gas-ranges of 10–100's, and 3000 ppbv, respectively, sufficient for using the low-cost electrochemical sensors to quantitatively investigate NO–NO_2–O_3 atmospheric chemistry. During four weeks in February–March 2021, sensors placed on the rooftop (20 m) and base (3 m) of a building in downtown Fairbanks identified strong gradients in atmospheric composition over a very short <20 m vertical scale at times when near-surface temperature inversions were present. At night, CO and NO_x were more concentrated at the surface than aloft, and surface ozone was depleted whilst sometimes being present aloft. During the daytime, when solar radiation heated the surface, inversions were disrupted by efficient vertical mixing that mixed in ozone-rich air from above. The low-cost sensor observations demonstrate that near-surface

[a]*LMD/IPSL, ENS, Université PSL, Ecole Polytechnique, Institute Polytechnique de Paris, Sorbonne Université, CNRS, Paris, France. E-mail: Tjarda.Roberts@lmd.ipsl.fr*

[b]*LPC2E, OSUC, Université d'Orléans, CNRS, CNES, 45071, Orléans, France*

[c]*Geophysical Institute and Department of Chemistry and Biochemistry, University of Alaska Fairbanks, AK 99775, USA*

† Electronic supplementary information (ESI) available: One supplementary material file. See DOI: https://doi.org/10.1039/d4fd00177j

pollutant trapping was correlated with thermal inversions and trace O_3–NO_x atmospheric chemistry, and quantify a local O_x source from direct "primary" NO_2 emissions, with a directly emitted $NO_2 : NO_x$ ratio of 0.13 mol mol^{-1}. The sensors also characterise NO_x emissions, finding a NO_x : CO of 0.15 mol mol^{-1}. When well-characterised, low-cost electrochemical sensors can provide valuable measurements of local emissions and vertically-resolved atmospheric composition, with sufficient accuracy to trace atmospheric chemistry in cold and stable wintertime urban environments.

Introduction

Observations of atmospheric composition in the Arctic are sparse yet particularly relevant in the urban Arctic due to local emissions.[1] Cities such as Fairbanks, Alaska, can experience severe air pollution episodes during winter, when enhanced local emissions, *e.g.*, from traffic and home heating,[2,3] become trapped near to the surface by temperature inversions.[4–7] Similar processes can also occur at lower-latitude basin and valley sites leading to episodes of severe wintertime air quality in locations such as Salt Lake Valley, Utah,[8] and Grenoble, France.[9] A stable temperature gradient inhibits mixing in the vertical, whilst sheltering by surrounding topography protects against mixing in the horizontal, leading to the development of persistent cold-air pools and the accumulation of surface air pollution.[10] The atmosphere above Fairbanks contains multiple thermal inversion layers during winter;[11,12] elevated inversion layers can occur up to several hundreds to thousands of meters aloft. Recent evidence highlights that very shallow inversions that develop at the surface or within tens of meters of the surface have an important role in downtown Fairbanks' air quality through trapping of surface emissions; Cesler-Maloney *et al.*[13] report vertical differences in particulate matter and ozone between the surface and 20 m aloft during surface-based inversions on similar vertical spatial scales, also supported by vehicle-based particle mapping.[14] These findings focus our attention on the atmosphere in tens of meters above Fairbanks, in which gradients in atmospheric composition can be unusually strong compared to lower latitudes. To better understand the causes of extreme enhanced surface pollution during Fairbanks wintertime, and associated chemistry and mixing processes affecting wintertime atmospheric composition, it is necessary to measure at such levels aloft as well as at the surface. However, many traditional instruments that quantify atmospheric composition are too demanding in their power consumption, weight or maintenance needs for this purpose. Furthermore, the Arctic presents a particular challenge to such instrumentation due to the very cold temperatures, which can reach as low as −40 °C during Fairbanks winter. This motivates our field-demonstration of low-cost, highly portable and low-power electrochemical gas sensors to continuously measure CO, NO, NO_2 and O_3 wintertime gas composition in the atmosphere above Fairbanks, Alaska.

Low-cost electrochemical sensing of air pollution and its potential for investigations of Arctic atmospheric composition

Over the last decade, networks of miniature electrochemical (amperometric) sensors have been applied to monitor surface air quality in low-latitude locations, *e.g.*, ref. 15–27. These studies mostly apply low-cost electrochemical sensors for

horizontal spatial mapping of surface air quality, or air pollutant exposure. Advantages of these sensors over traditional atmospheric instrumentation include their low power requirement and low cost (0.01 watts and about a hundred euros per sensor). One small instrument (hundreds of g up to a few kg) can house multiple electrochemical sensors alongside other small gas and particle sensors and data-acquisition electronics. Commercial sensor packages (at a cost of several thousand euros) typically do not require specialist installation, and can deliver fully autonomous monitoring of multiple pollutant gases over many months with quasi real-time transfer of the measurements to a data-cloud. These advantages facilitate the deployment of multi-sensor monitoring networks, applications on mobile platforms, *e.g.*, ref. 15, or in remote locations, *e.g.*, ref. 25 and 27. However, sensor accuracy, biases and drift can be significant limitations, *e.g.*, ref. 23 and 24, and are the main disadvantages of low-cost electrochemical sensors compared to traditional instruments. These limitations tend to become critical at low gas abundances and thus are particularly pertinent in research investigations of atmospheric chemistry, where ozone varies by just tens of ppbv.

Indeed, few studies have exploited low-cost electrochemical sensors to investigate atmospheric chemistry, which requires robust ppbv-level detection of gases such as NO, NO_2, and O_3. A consistent sensor performance with ppbv-level accuracy is also required to quantify vertical differences in atmospheric composition over time. Here, we deploy two sets of well-calibrated sensors to demonstrate low-cost electrochemical sensing of atmospheric composition at the ppbv-level over weeks to months in the urban Arctic atmosphere. We thereby trace O_3–NO–NO_2 atmospheric chemistry and quantify vertical differences in wintertime CO, NO, NO_2 and O_3 composition of the atmosphere over very short vertical scales (3 m to 20 m) above Fairbanks, Alaska.

Vertically-resolved measurements of atmospheric gas composition are needed during surface pollution episodes

In Arctic cities such as Fairbanks (and some lower-latitude urban environments), the occurrence and severity of wintertime surface pollution episodes depends crucially on the degree and scale of the vertical mixing. Episodes of poor air quality are more severe when local emissions become trapped and accumulate near to the surface, and less severe when the emissions can disperse and dilute in the vertical. As recently highlighted,[13,14] near-surface thermal inversions have a critical role in the trapping of locally-emitted pollutants very close to the surface, leading to severe air-quality episodes in Fairbanks. Under calm winds, such inversions can develop during the cold Arctic night, but can be disrupted by daytime solar heating of the surface during Fairbanks late-winter (February to March), causing enhanced vertical mixing and dilution of the surface pollution. Atmospheric chemistry furthermore influences the composition of the wintertime atmosphere. For example, reaction cycles involving ozone control the partitioning between NO and NO_2 in NO_x, and can convert NO_x into nitrate particulate matter through photolytic oxidation and non-photolytic mechanisms (the latter may have particular relevance in Fairbanks' dimly-lit winter[13]). Such chemical reactions progress as a function of the concentrations of pollutants and oxidants, *e.g.*, ozone, and depend on the composition of the local emissions and also on how

vertical mixing distributes pollutants and may promote chemical reactions through in-mixing of cleaner and more ozone-rich air masses from aloft.

This study investigates the vertical distribution in atmospheric composition above Fairbanks, Alaska. We demonstrate continuous monitoring of atmospheric CO, NO, NO_2 and O_3 abundances by low-cost electrochemical sensors at two heights (at 3 m and 20 m by sensor rooftop deployment) during a four-week period in February–March 2021. We correlate these measurements to inversions traced by temperature sensors on a 11 m mast. We quantify vertical gradients in atmospheric composition across the diurnal cycle. We relate the sensor observations to trapping of locally emitted pollutants by night-time inversions, enhanced vertical mixing during the daytime, and atmospheric chemistry. Using low-cost electrochemical sensors, we also characterize local Fairbanks emissions with a focus on CO, NO_x, and O_x (signifying primary NO_2) emissions.

Methods

Low-cost electrochemical sensing of CO, NO, NO_2 and ozone

Two sets of four miniature electrochemical gas sensors (CO-A4, NO-A4, NO2-A43F and Ox-A431, Alphasense Sensor Technology Company) were used to measure CO, NO, NO_2 and O_3 at 0.1 Hz with data hourly-averaged for the purpose of this study. The cm-sized electrochemical sensors were housed with the downward-facing diffusion face exposed directly to the air within two identical mains-powered instruments (EMSOL Praxis Unit, originally by SouthCoastScience), that co-measured the sensor temperature (Sensirion SHT3x), and transferred sensor signals to a data cloud *via* a 4G cellular phone modem in near real-time. For each target gas, the raw electrochemical sensor signal (S, working electrode current, recorded as voltage *via* 0.8 mV nA^{-1} gain of the Alphasense AFE electronics) was analysed to extract mixing ratios [X, ppbv], by rearranging the sensor equation, *e.g.*, ref. 28, $S = B + s_X \cdot [X]$, where the baseline (B, volts) and sensor sensitivity (s, volts $ppbv^{-1}$) are sensor-specific and temperature dependant, and were calibrated by cross-comparison to air-quality monitoring data. As the Ox-A431 sensor is sensitive to both ozone and NO_2, the measurement of ozone required subtraction of the interference of NO_2 (cross-sensitivity cs_{NO_2} multiplied by NO_2 mixing ratio, *i.e.*, $cs_{NO_2} \cdot [NO_2]$) from the Ox-A431 sensor signal, S_{O_3}, (see **https://www.alphasense.com/** and ref. 29). The other sensors exhibited negligible inter-gas cross-sensitivities. The cross-comparison calibrations to air-quality reference monitors were undertaken at the NCORE site during two periods, from January 7th to February 7th 2021, and from 9th March to 31st March 2021. The NCORE site is an air-quality monitoring site located in downtown Fairbanks operated by the ADEC (Alaska Department of Environmental Conservation). A range of reference monitors for gases and particulate matter are operated within heated trailers at NCORE, delivering air-quality datasets that are publicly available from the DEC website and contribute to the US Environmental Protection Agency monitoring network. The NCORE gas-monitoring system was upgraded in 2020. This study uses NCORE datasets from the CO analyser (Teledyne API T300U), NO and NO_y analyser (Teledyne T200U) and ozone analyser (Thermo 49iQ), supplied as hourly averages alongside ambient temperature. NO_2 was not directly measured by the DEC at NCORE in 2021. An indirect DEC measurement of NO_2 is

approximated by NO_2 = NO_y–NO. This approximation is appropriate for the polluted conditions of downtown Fairbanks, as demonstrated by intercomparison of NO_x and NO_y instruments deployed by the DEC at NCORE during previous winters (ESI Fig. S1†). During January–March 2021, the DEC ozone analyser at NCORE experienced some issues in drifting baseline stability, leading to data gaps and uncertainty in the reported values. We address this uncertainty by comparing the provisional NCORE ozone data provided by the DEC to data from another ozone monitor (Dasibi 1008-RS O_3 photometric analyzer) that was deployed in a heated trailer at the nearby CTC site (~500 m distance) during February 2021 to deliver a corrected surface ozone measurement (ESI, Fig. S2†).

Field campaign: atmospheric composition measured at two heights (3 m and 20 m) in downtown Fairbanks

To probe vertical differences in Fairbanks' air composition, the sensors were deployed at two heights at the CTC site from 7th February to 9th March 2021. The CTC site is located about 500 m south from the NCORE site, in downtown Fairbanks. At 20 m high, the CTC (University of Alaska Community Technical College) is one of the tallest buildings in Fairbanks. One set of sensors (Praxis 430) was deployed on the CTC roof at about 20 m above ground, the other (Praxis 429) was deployed on top of a trailer at the CTC base, approximately 3 m above ground. These two-height gas measurements of CO, NO, NO_2, and O_3 were complemented by measurements of the inversion strength over the 4-week period. Ambient temperature at 11 m and 3 m height was measured on a mast near to the CTC building (with aspirated thermocouples[13]), enabling derivation of the 11–3 m temperature difference. Ambient temperature was not measured at 20 m on the CTC roof, but the temperature of the electrochemical sensors was monitored, from which a 20–3 m T_{sens} sensor temperature difference can be derived.

Results and discussion

Low-cost electrochemical sensing of atmospheric composition (CO, NO, NO_2 and O_3) in downtown Fairbanks

Time-series from the two sets of four low-cost electrochemical sensors for CO, NO, NO_2 and O_3 that were deployed in downtown Fairbanks, at the NCORE site (3 m) for the cross-calibration to air-quality analysers (shaded region, 7 Jan–7 February and 9 March–31 March, 2021), and at the nearby-located CTC site (3 m) and CTC building roof (20 m) for measuring vertical gradients (unshaded region, 7 February–9 March 2021) are shown in Fig. 1a. Sensors were deployed continuously, with hourly averages presented in this study. Fig. 1a demonstrates that the sensors exhibited negligible drift over the three-month period. An estimate of sensor accuracy is given in Table 1, which presents the analysed sensor output compared to that of air-quality analysers in terms of R^2, RMSE or root-mean-square error, and mean absolute error, where alternate hourly data has been used in the cross-calibrations and statistical analyses (n > 500 data points for each, across the total cross-comparison period). From this evaluation, the mean absolute errors are < 50 ppbv (CO) and < 5 ppbv (NO, NO_2, O_3). This lends confidence to the field-campaign measurements at the CTC site (unshaded region, 7 February–9 March 2021) when significant differences in measured air composition can be

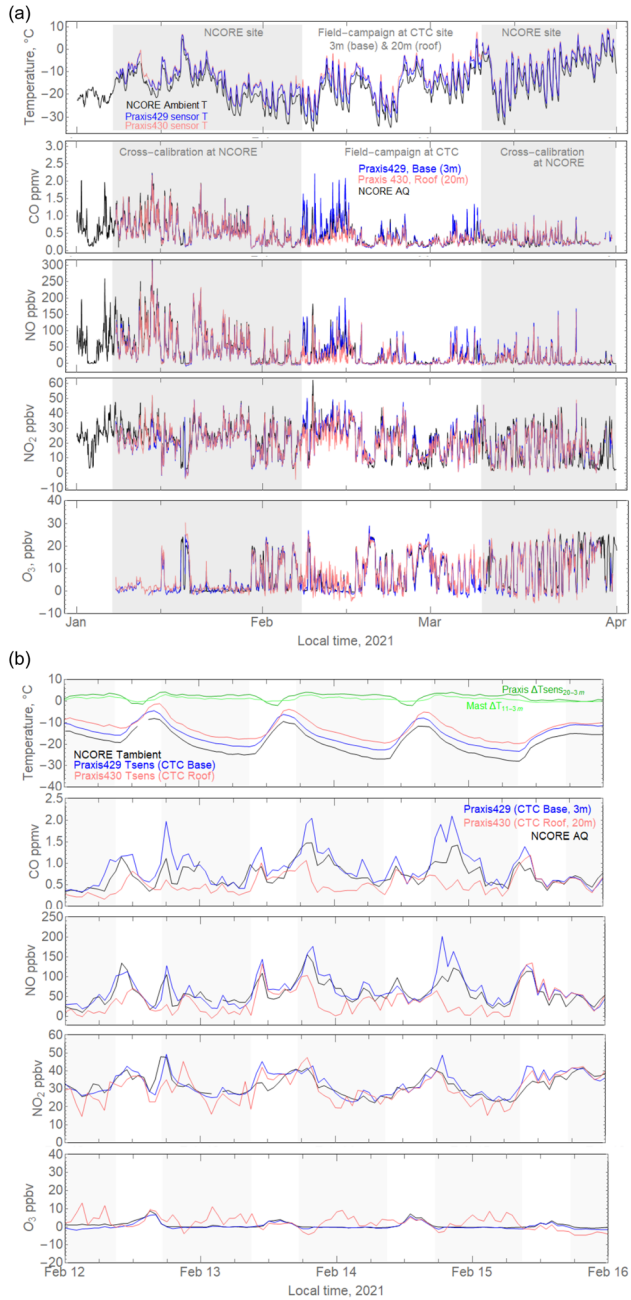

Fig. 1 (a) Time-series of hourly CO, NO, NO_2, and O_3 gas abundances measured by low-cost electrochemical sensors in two instruments (Praxis 430, pink, and Praxis 429, blue) in downtown Fairbanks. Also shown are measurements by DEC air-quality monitors (black) at the Fairbanks NCORE EPA monitoring site. During January 9–February 7 and March 9–March 31, the sensors were co-located at NCORE (3 m), shaded regions, as part of cross-calibration. During February 7–March 9 the sensors were located at the CTC site (500 m south of NCORE) at the base (3 m height, Praxis 429, blue) and on the CTC building rooftop (20 m height, Praxis 430, pink), and show distinct differences in air composition.

seen between the 20 m rooftop and 3 m surface air during surface pollution events. During January to March, Fairbanks typically experiences the transition from being dimly-lit with severe surface air pollution to a very strong diurnal solar cycle, and less severe and more variable surface air pollution conditions. The ambient temperature generally warms during these months, but with substantial temporal variability (ranging from below −30 °C to above 0 °C during January–March 2021). Furthermore, from February onwards, and depending on local meteorological conditions, surface heating by solar radiation can cause strong diurnal temperature changes, which sometimes exceed 10 °C, as was observed during the Fairbanks winter of 2021 (Fig. 1a). Near-surface wind-speeds were low (averaging around 0.5 m s^{-1}, data not shown), confirming calm conditions suitable for the development of thermal inversions. During the CTC field-campaign (7 February–9 March 2021), the low-cost-sensor measurements show that pollution was more enhanced at the surface (3 m) than aloft (20 m), particularly during the periods with ambient temperature minima. Such strong vertical gradients in atmospheric composition indicate near-surface trapping of local pollutants by thermal inversions at night.

Strong vertical gradients in atmospheric composition 20 meters above Fairbanks in February 2021

The mid-February period that exhibits strongest vertical differences in the two-height (20 m and 3 m) atmospheric composition measurements is highlighted in Fig. 1b (where light shading denotes darkness, unshaded is sunlit). Surface NO and CO become enhanced in the evening just after dusk, reaching 2 ppmv and 100–200 ppbv, respectively, at the CTC base. There is also a smaller peak in these pollutants in the mid-morning. The maxima in these pollutants, CO and NO, are significantly lower on the CTC roof, by approximately a factor of two or more. The measured NO_2 exhibits these same early-evening and mid-morning maxima, but NO_2 abundance is more similar at all sites, sometimes just slightly (~10 ppbv) lower at the roof at night. The range in NO_2 is between 20 and 50 ppbv, and the trend at all sites is typically decreasing during the night (after the evening NO_x peak) and increasing in the morning. Ozone exhibits an opposing and complementary trend to NO_x (NO + NO_2). During the night, ozone becomes enhanced at the CTC roof at 10–15 ppbv, whilst it is low and near-zero at the surface. During the day (late morning), surface ozone increases. By mid-afternoon, ozone reaches

Also shown is the ambient temperature monitored at NCORE (3 m) and sensor temperatures that are slightly (~5 °C) above ambient. (b) Hourly CO, NO, NO_2, and O_3 measured by two sets of low-cost electrochemical sensors at two heights: CTC base at 3 m (Praxis 429, blue) and on the CTC building roof at 20 m (Praxis 430, pink). Also shown is surface (3 m) air-quality monitoring data (black) from the nearby NCORE site. Shaded/unshaded denotes night/day. Data is as in Fig. 1a, here with a zoom on the February 12 to February 16 period, which exhibits the strongest night-time trapping of pollutants as observed from the two-height measurements. Ozone exhibits an inverse trend with cleaner air aloft during the night. Also shown are the ambient temperature at NCORE, and the sensor temperature of the two Praxis instruments. In addition, the first panel shows vertical differences in the measured temperature of the low-cost sensors (20–3 m) and of ambient temperature measured by thermocouples on a nearby mast (11–3 m), which denote the presence of night-time inversions.

Table 1 Statistics of the two electrochemical sensor sets (Praxis 430 and Praxis 429) compared to ADEC air-quality monitors when co-located at the NCORE EPA monitoring site in downtown Fairbanks (7 Jan–7 February and 9 March–31 March, 2021, shaded regions Fig. 1a), across sensor temperatures $-30\ °C \leq T_{sens} \leq 0\ °C$. RMSE: root-mean-square error. MAE: mean absolute error. Analysis and calibration are performed on alternate data points ($n > 500$ each) during this cross-comparison period to enable statistics on the sensor gas measurement independent from the data used for sensor calibration

Sensor set	Sensor type	Target gas	Max ppbv	R^2	RMSE ppbv	MAE ppbv
P430	CO-A4	CO	2243	0.96	70	45
	NO-A4	NO	327	0.98	6.9	4.2
	NO2-A43F	NO_2	51	0.88	3.5	2.6
	Ox-A431	O_3	27	0.90	3.0	2.0
P429	CO-A4	CO	2001	0.95	69	47
	NO-A4	NO	252	0.98	7.2	4.6
	NO2-A43F	NO_2	44	0.86	3.5	2.6
	Ox-A431	O_3	27	0.94	2.1	1.4

a uniform vertical distribution at 5–10 ppbv at all sites, marking the diurnal maximum surface abundance and only a local rooftop maximum. These diurnal patterns and vertical gradients in CO, NO_x and ozone can be readily qualitatively interpreted as the combined effects of local emissions (with early-evening and mid-morning maxima), pollution trapping by thermal inversions that develop during the night and inhibit vertical mixing, disruption of the inversions by solar heating during the day leading to strong vertical mixing, and atmospheric chemistry that interconverts NO, NO_2 and O_3.

The following sections discuss these aspects and present their characterisation or quantification through further analysis of the low-cost electrochemical sensor measurements over the whole 7 February–9 March two-height field-campaign period.

Low-cost sensing of O_3–NO–NO_2 atmospheric chemistry

Atmospheric chemistry exerts a strong control over the O_3–NO–NO_2 ppbv mixing ratios that is accurately captured by the electrochemical sensors: ozone and NO_2 show an inverse relationship across the instrument time-series (Fig. 1a and b). Reactions (R1)–(R3) interconvert NO and NO_2 on a timescale of minutes under sunlit conditions.

$$NO + O_3 \rightarrow NO_2 + O_2 \quad \text{(R1)}$$

$$NO_2 + h\nu \rightarrow NO + O(^3P) \quad \text{(R2)}$$

$$O(^3P) + O_2 + M \rightarrow O_3 + M \quad \text{(R3)}$$

The dynamic relation between the observed NO, NO_2 and ozone is illustrated in Fig. 2 (dimly daylit, and dark hours) for the measurements at NCORE, the CTC base and the CTC roof during February 7th to March 9th. The sensors and AQ monitors show similar results, which reflects good instrument functioning

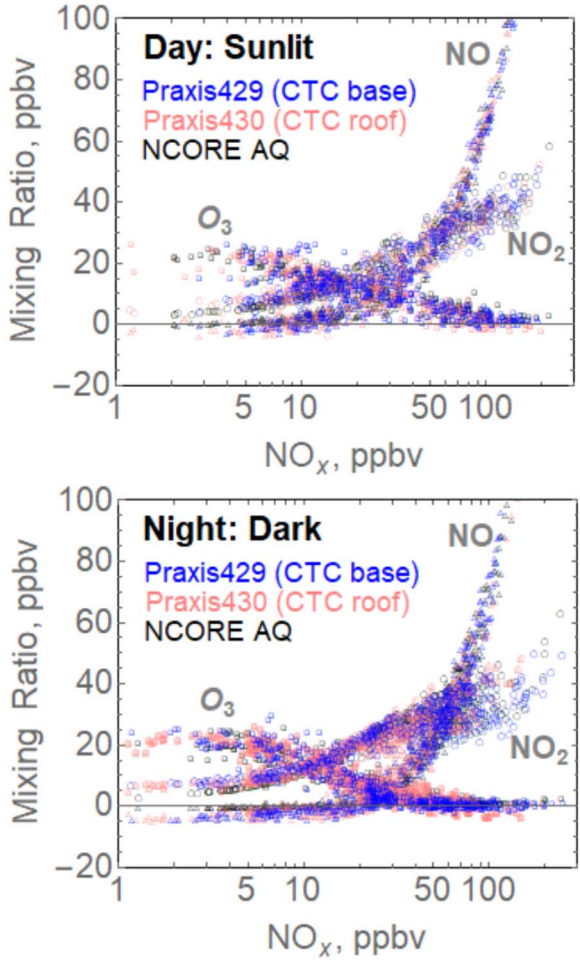

Fig. 2 Low-cost electrochemical sensing of the atmospheric chemistry relationship between NO, NO_2 and O_3 to NO_x ($NO + NO_2$) as measured during the day and night during the field campaign (7 February–9 March 2021) in downtown Fairbanks. Sensors were located at 20 m height on the CTC roof (P430 sensor set, pink) and at 3 m on the CTC base (P429 sensor set, blue). To validate the ppbv-level low-cost electrochemical sensor measurements, a comparison is made to NO, NO_2 NO_x and O_3 measured by air-quality monitors at the Fairbanks NCORE site (black), 500 m north of the CTC site. Note the log scale for the *x*-axis.

(notwithstanding uncertainties in the span of the air-quality monitor for ozone; see Methods). When NO_x exceeds ~50 ppbv, ozone is depleted and NO and NO_2 are enhanced. Despite the dimly-lit Fairbanks winter conditions, a dynamic equilibrium between NO, NO_2 and ozone can readily establish during the sunlit daytime. The solar noon lifetime for NO_2 at Fairbanks' latitude and longitude on 21 February is 6.1 minutes (Tropospheric Ultra-Violet and Visible Radiation Model v5.3 (ref. 30)), even without considering the effects of enhanced albedo due to surface snow. During the night, suppression of NO_2 photolysis leads to slightly higher NO_2 and lower NO and ozone compared to the day (Fig. 2).

Thermal inversions, vertical mixing and emission trapping

Temperature differences between surface and aloft. Near-surface inversions can be quantified from hourly temperature differences between the surface (3 m) and aloft, using the mast-based aspirated thermocouple temperatures, T_{mast}, at 3 m and 11 m. We also calculate the differences in measured temperature of the electrochemical sensors, T_{sens}, at 3 m and 20 m, but that are subject to heating from the local instrument-environment, estimated at around 5 °C above ambient temperature based on comparing the 3 m CTC base and 3 m mast temperatures (T_{sens}–T_{mast}) (Fig. 3 upper). Analysis of vertical gradients in temperature (T_{mast} 11–3 m and T_{sens} 20–3 m divided by the vertical distances of 8 m or 17 m,

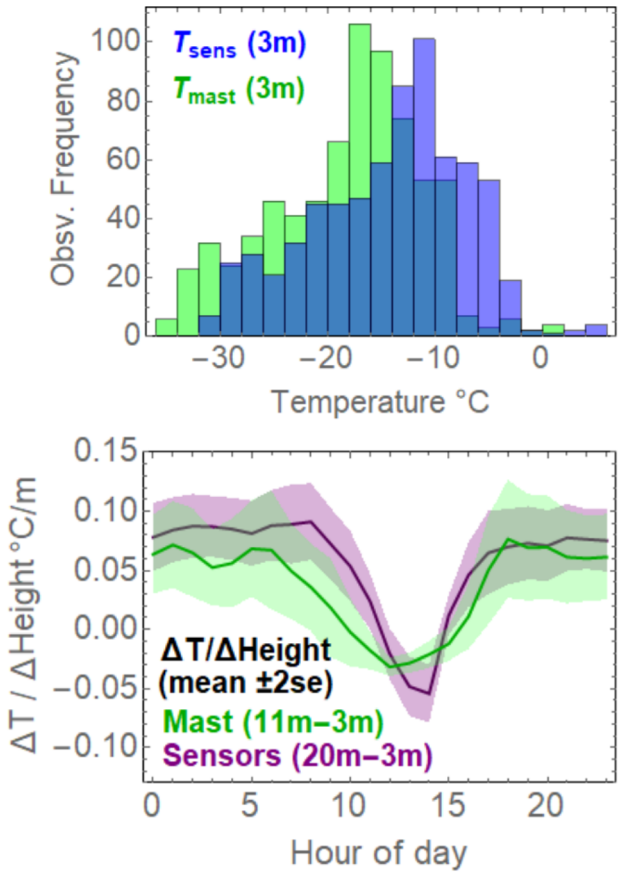

Fig. 3 Upper: Histogram of hourly temperature measured at 3 m on the mast (T_{mast}, green) and the sensor temperature in Praxis P429 (T_{sens}, blue) showing consistent ~5 °C instrument warming of T_{sens} compared to ambient T as measured on the mast during the field campaign. Lower: Diurnal cycle in hourly temperature gradient (temperature difference divided by height difference) measured using aspirated thermocouples over 11–3 m on the mast (green) and by the Praxis instrument gas sensor temperatures over 20–3 m from CTC roof to surface (purple), indicating the two methods show consistent trends and measured magnitudes of the night-time inversions, with some additional instrument-heating effects on gas sensor temperature during the day.

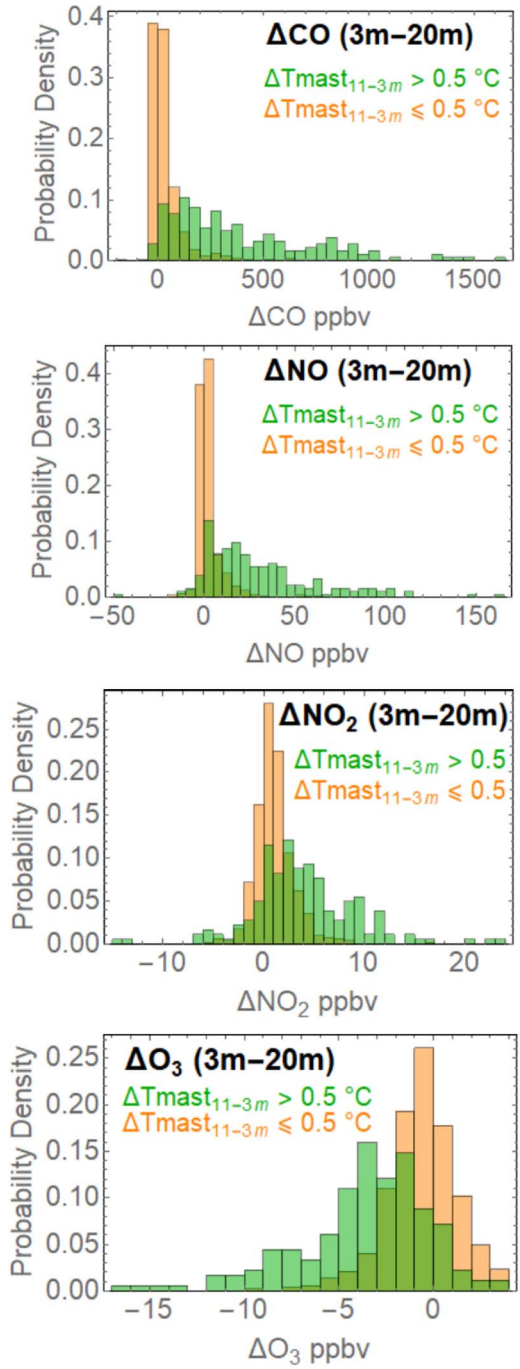

Fig. 4 Probability histograms of the vertical difference (3–20 m) in hourly gas abundances measured between the CTC surface and roof during the 7 February–9 March 2021 downtown Fairbanks field-campaign. Data is categorised above and below a 0.5 °C threshold for the vertical 11–3 m temperature differences co-measured on the nearby mast, as a measure of the presence (green) or absence (orange) of strong inversions, following Cesler-Maloney *et al.*[13]

respectively) finds a strong diurnal variation (Fig. 3 lower). Both T_{mast} and T_{sens} methods observe strongly stably stratified conditions during the night, with average temperature gradients above +0.05 °C m^{-1} (*i.e.*, nearly 1 °C between surface and rooftop developing on average each night). During the daytime this positive gradient declines to unstable/neutral conditions, reflecting warming of the near-surface air through solar heating of the surface. The local solar noon is around 13 h to 14 h in Fairbanks, with peak surface temperature around 15 h. The diurnal cycle derived from T_{sens} is somewhat skewed compared to the cycle from the mast T, and the T_{sens} daytime minimum substantially overshoots the adiabatic lapse rate (−0.0098 °C m^{-1}), likely reflecting slight differences in heating of the two instruments and their gas sensors during daytime surface warming. The 20–3 m T_{sens}-derived and 11–3 m T (mast)-derived temperature gradients are nevertheless in quantitative agreement during the night. In the following, we used mast (11–3m) T differences and a scaling factor (20–3)/(11–3) = 17/8 to estimate temperature differences between the CTC roof and surface, for comparison to the measured vertical differences in pollutants between roof and surface.

Pollutant trapping <20 m by near-surface thermal inversions. A histogram approach is used to present differences in roof and surface pollution abundances (Fig. 4). Data is categorised according to mast-based 11–3 m temperature differences above and below a threshold of 0.5 °C, which was proposed by Cesler-Maloney *et al.*[13] as an indicator of strong inversions causing near-surface pollution trapping during the 2019–2020 winter. The 7 February–9 March 2021 dataset supports this choice of threshold: vertical differences in CO, NO, NO_2 and O_3 are close to zero (just slightly enhanced at the surface by few ppbv) for $T_{11m-3m} \leq$ 0.5 °C, whereas for T_{11m-3m} > 0.5 °C the vertical differences are strongly skewed due to the near-surface trapping of pollutants by inversions, resulting in enhanced surface abundances of CO, NO and NO_2, and lower surface abundances of O_3 compared to those at 20 m. The NO_2 distribution shows a more subtle pattern than CO or NO, as it also reflects the compensating role of atmospheric chemistry in converting NO into NO_2 where ozone is available, therefore exhibiting a surface enhancement, but is more evenly distributed between surface and rooftop.

The relationship between the roof-to-surface temperature difference (using 11–3 m mast data scaled to represent 20–3 m roof–surface differences; see above) and the roof-to-surface pollution difference is further quantified through scatter plots: Fig. 5 shows the hourly vertical differences in pollutants *versus* hourly vertical differences in temperature for CO, NO, NO_2, O_3 and also NO_x (NO + NO_2) and O_x (NO_2 + O_3). The near-surface locally emitted pollutants CO, NO and NO_x exhibit strong positive correlations between enhanced surface abundance (relative to the rooftop) and greater temperature stability. Under the most stable conditions (higher temperature difference between roof and surface), the magnitude in the vertical difference in these pollutants is most variable: very large differences may reflect periods with high emission fluxes under prolonged strongly stable conditions, leading to substantial CO, NO or NO_x pollutant accumulation at the surface. NO_2 and O_3 exhibit opposing trends that are generally more linear, reflecting their interconversion by atmospheric chemistry. The calculated linear regressions on vertical rooftop-to-surface differences in NO_2 and O_3 with vertical difference in temperature are approximately equal at ±0.8

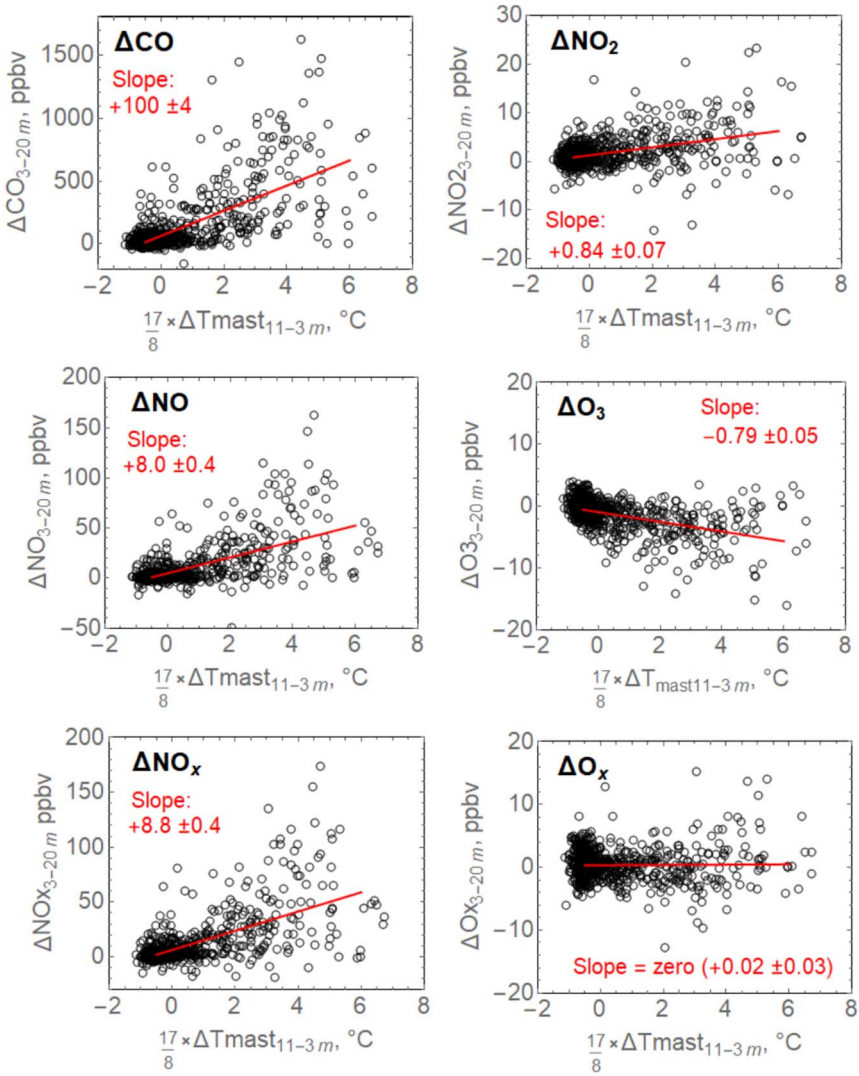

Fig. 5 Scatter plots of vertical differences in gas abundance (at height: 3–20 m) *versus* vertical difference in temperature (mast 11–3 m scaled by (20–3)/(11–3) = 17/8, to be equivalent to the temperature difference over 20–3 m height). Note that this specific choice of axes gives positive trends for a greater near-surface trapping of pollutants (*y*-axis) with stronger thermal inversion (*x*-axis). Left-hand-column plots show positive (non-linear) trends for CO, NO and NO_x. Right-hand-column plots show a positive linear trend for NO_2, a negative linear trend for O_3 and no trend for O_x. Linear fits are presented for all species, with slopes quantified.

ppbv per °C (calculated over 20–3 m). The corresponding trend in O_x ($NO_2 + O_3$) is approximately flat, with the vertical O_x difference being around zero. This is expected given the near-equal and opposite gradients in NO_2 and O_3. Processes that can form/destroy O_x or emission sources of O_x were comparatively small or more

subtle during the field-campaign period, and are investigated through a diurnal data analysis below.

Diurnal changes in atmospheric composition at the surface and 20 m above Fairbanks

Diurnal trends in the surface (3 m) and rooftop (20 m) abundances of CO, NO, NO_x and NO_2, and O_3 and O_x as well as their vertical differences (3–20 m) are shown through their hourly mean and standard error during the field campaign (7 February to 9 March 2021) (Fig. 6). As a data quality check, differences between these sensors are also calculated for the 9 March–31 March period, when they were co-located at 3 m at NCORE, confirming that potential diurnal biases are very small (few ppbv) (ESI Fig. S3†). The diurnal temperature gradient during the 7 February to 9 March 2021 field campaign (Fig. 4, lower) quantified

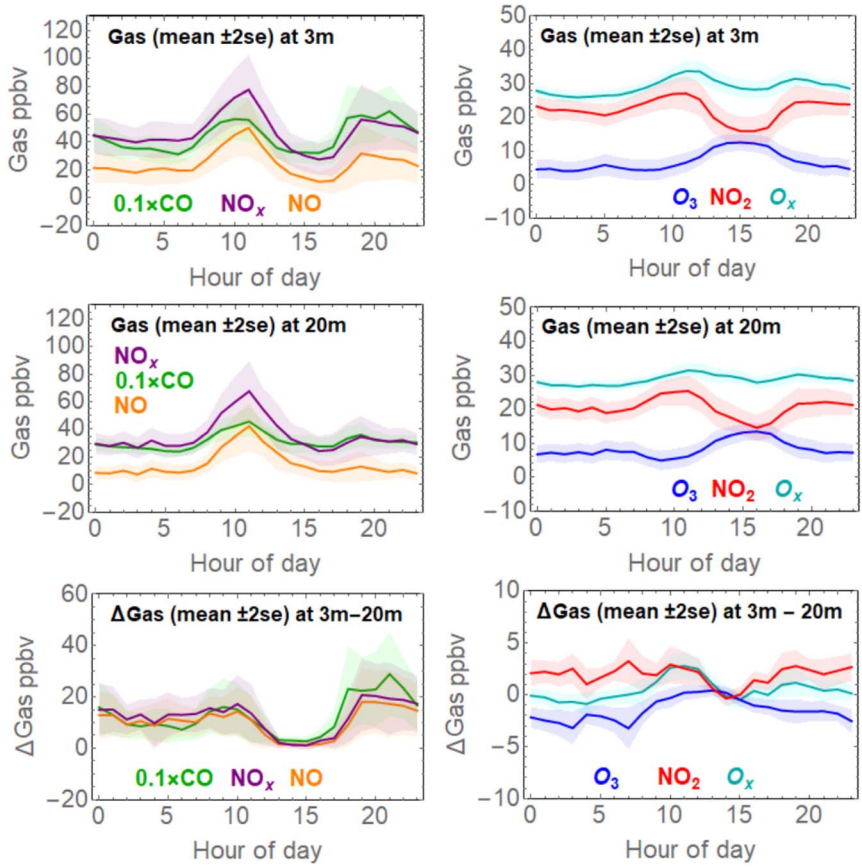

Fig. 6 Diurnal variation in the hourly mean (line) ± 2 standard errors (shaded region) gas composition measured by low-cost electrochemical sensors at the CTC base (3 m) and CTC roof (20 m), and vertical difference (3–20 m) during the 7 February–9 March 2021 field campaign in downtown Fairbanks. The left-hand column shows CO/10 (green), NO_x(purple) and NO (orange). The right-hand column shows NO_2 (red), O_3 (dark blue) and O_x (light blue). Hour is local hour from 0 to 23.

the inversions with strongly stable conditions that enhance pollutant trapping during the night, but are disrupted during the daytime to enable efficient vertical mixing during the afternoon. Another factor controlling the diurnal pollutant abundances, their trends and vertical differences is the diurnal variation in local emissions. Inspection of Fig. 6 can enable to qualitatively detangle these two convoluted effects and identify key controls on Fairbanks' surface and near-surface atmospheric composition. Hourly mean CO, NO and NO_x surface pollution exhibits twice daily maxima in the mid-morning (10–11 am) and early evening (7–8 pm), with a daily minimum around 3 pm, and similar variations are seen for NO_2 over a much smaller ppbv scale. Conversely, for the rooftop data only the morning pollution maximum is clearly evident. The vertical differences confirm that efficient trapping of early-evening emissions below 20 m is responsible for surface night-time pollution, whereas the morning emissions yield similar surface abundances but mix up to higher heights, to (above) 20 m. This suggests a particularly strong mid-morning emission flux that is also more NO_x-rich than in the evening. Nighttime ozone shows the inverse behaviour to NO_2 with lower ozone at the surface ($\sim$5 ppbv) than aloft ($\sim$10 ppbv). This is due to ozone titration by reaction with NO, which occurs at both levels but to a greater extent at the surface where NO_x is most abundant. The measured vertical difference in ozone is eroded during the morning, concurrent with NO_x emissions partially mixing up to 20 m. Subsequently, in the mid-afternoon, ozone becomes enhanced at both the surface and at 20 m to around 15 ppbv at 3-4pm. This indicates an efficient vertical mixing that brings down ozone-rich air from further aloft. Concurrently, both the surface and rooftop pollutant abundances (CO and NO_x) diminish. The atmosphere is measured to be vertically uniform in CO, NO, NO_2, and O_3 composition between 3 and 20 m at around 14–15 h. Pollutant abundances then increase (and ozone decreases) as the sun sets and thermal inversions can develop again to trap the local emissions. O_x abundances are broadly similar at the rooftop and surface as previously noted, but the diurnal trend in O_x is not flat. At the surface (and to a lesser extent on the rooftop), O_x is enhanced during the morning and evening emission peaks, particularly in the mid-morning when NO_x is most enhanced, also highlighted by the vertical difference in O_x. This suggests a local emission source of O_x as well as NO_x that is further characterised and quantified below. It has also been hypothesized that O_x loss processes may occur in the atmosphere above Fairbanks during the night, *via* NO_3–N_2O_5 chemistry to form nitrate under moderately polluted and dark conditions when ozone and NO_2 are present.[13] Such processes are difficult to elucidate using this hourly-averaged two-height dataset but are being investigated with higher time resolution data, including ALPACA 2022 Fairbanks campaign measurements by low-cost electrochemical sensors.

Characterising Fairbanks emissions using low-cost sensors

Fairbanks NO_x emissions. NO_x has a key role in atmospheric chemistry and NO_2 is an important regularised component in air-quality monitoring. However, unlike for CO and particles, NO_x emission data is limited for Fairbanks, and may be underestimated.[31] NO_x emissions are evident in Fig. 6 during both the morning and evening. Comparison of the CO and NO_x (NO + NO_2)

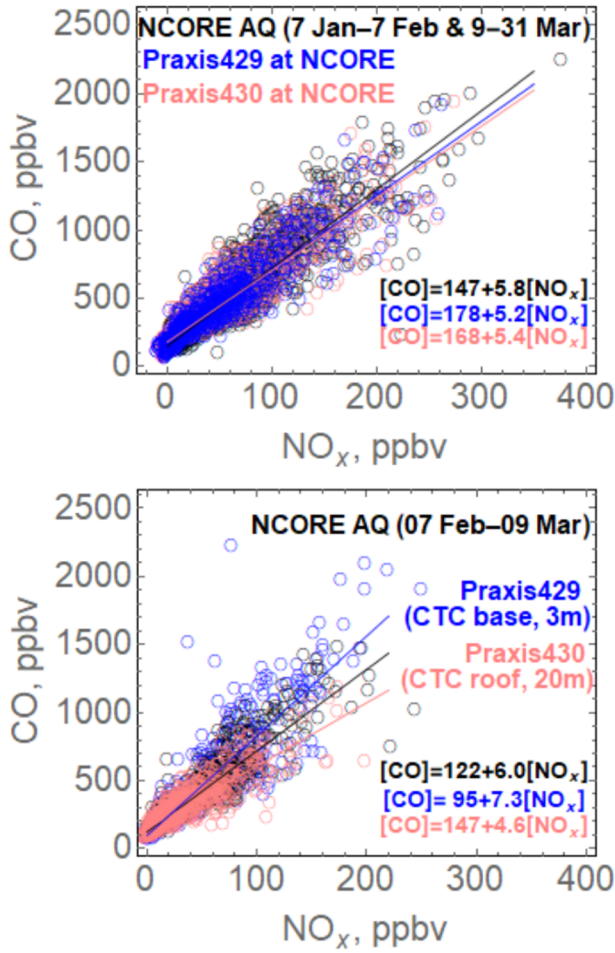

Fig. 7 Scatter plot of hourly CO (ppbv) *versus* NO_x (NO + NO_2, ppbv) measured by low-cost electrochemical sensors in Fairbanks, at the NCORE site (7 Jan–7 Feb and 9 Mar–31 Mar 2021, P430 in pink and P429 in blue), and at the CTC site (7 Feb–9 Mar, P430 at 20 m on the rooftop in pink, P429 at 3 m at the CTC base in blue), shown in the upper and lower plots respectively. Shown alongside are hourly data from air-quality analysers at NCORE for the same periods (black). Linear regressions are calculated for each dataset, with the gradient quantifying the CO : NO_x ratio under polluted conditions at each location and the intercept providing an estimate of the background CO mixing ratio at low NO_x conditions.

ratios measured at NCORE, the CTC base and the CTC roof enables characterisation of the local NO_x emissions (Fig. 7). Linear regressions find that the measured CO/NO_x ratios (5.2 to 5.8 ± 0.1 mol mol^{-1}, equivalent to 0.15 ± 0.01 mol mol^{-1} NO_x/CO) are in good agreement between all instruments when located at NCORE (*i.e.*, sensor algorithm fitting period in January and March). When the sensors were located at the CTC roof and base during February, the measured CO/NO_x ratios are also broadly similar, at 4.6 to 7.3 (±0.1) mol mol^{-1}. The CO *versus* NO_x data clouds from the low-cost sensors and NCORE analysers strongly overlap at moderate pollution levels (<100 ppbv NO_x or 500 ppbv CO).

The spread in CO/NO_x is more evident for the few observations at higher pollution levels. This likely reflects a combination of variations in local emissions (*e.g.*, traffic, home heating) over time and location as a function of source mixes and temperatures (*e.g.*, as seen in Fig. 6 diurnal means) as well as instrument uncertainties. Higher CO/NO_x at the CTC base may be expected, as it is geographically more exposed to CO-rich road traffic emissions. The CTC is also surrounded by a slightly greater density of homes. Finally, we note the regression lines in Fig. 7 yield intercepts (95–180 ppbv) consistent with the CO tropospheric background.

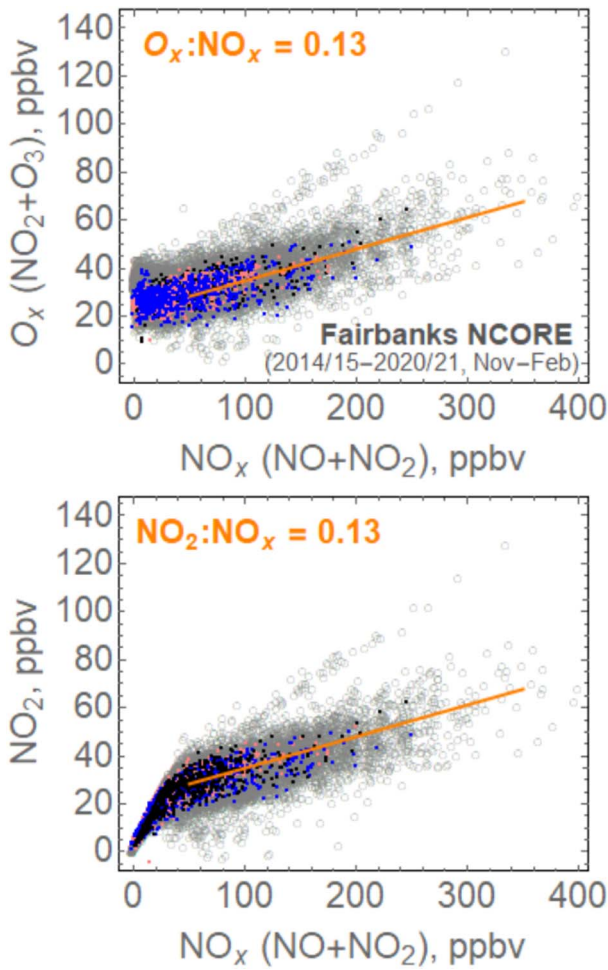

Fig. 8 Hourly O_x (O_3 + NO_2) *versus* NO_x (NO + NO_2) and NO_2 *versus* NO_x measured by electrochemical sensors during the field campaign (P430 in pink, P429 in blue, measured at the CTC roof and base, respectively; see the caption of Fig. 7), and measured by air-quality monitors at NCORE during the field campaign (black) and during the six preceding winters November–February from 2014–15 up to 2020–21 (gray open circles). The average O_x : NO_x and NO_2 : NO_x emission ratios are calculated using NCORE data with NO_x > 50 ppbv.

A source of O_x in Fairbanks. During the 2021 winter, O_x co-varied by 10's of ppbv at NCORE, the CTC base and the CTC roof (Fig. 8). In all periods and sites, maxima in O_x (NO_2+O_3) tend to be accompanied by high NO_x (NO + NO_2), *e.g.*, Fig. 1b and 6. As reactions (R1)–(R3) conserve O_x (the sum of NO_2 and ozone), other processes must be responsible for the observed variations in O_x. Sources of O_x are particularly pertinent during the darkest Fairbanks winter months when slow photolysis limits the formation of oxidants, and ozone is typically titrated by high NO emissions. The correlation between O_x (as NO_2) and NO_x identified by the low-cost sensors is confirmed by analysis of NCORE air-quality monitoring datasets over seven Fairbanks winter seasons (November to February, 2014–2015 to 2020–2021) (Fig. 8). The multi-year average $O_x : NO_x$ ratio is 0.13 mol mol^{-1} (calculated on all data where NO_x > 50 at NCORE, with a range of 0.12–0.15 mol mol^{-1} for the individual winters, except 0.06 mol mol^{-1} in 2019–2020). The NO_x-dependent source of O_x is observed across all dimly-lit and dark Fairbanks winter months, thus likely reflecting a 'primary' or 'direct' emission of NO_2, rather than a photochemical origin. A possible emission source is vehicular primary emissions of NO_2. Our observed NO_2/NO_x of 0.13 mol mol^{-1} in Fairbanks is within the range reported by studies of European road traffic,[32] but is more than double the ratio of 0.053 mol mol^{-1} found in a study of US road traffic in Denver Colorado.[33] The high NO_2/NO_x is somewhat surprising: vehicular traffic is typically gasoline-dominated in the United States in contrast to Europe where diesel fuel is largely responsible for high NO_2 emissions. Alaskan cities such as Fairbanks may have a higher proportion of diesel vehicles than cities in other US states. Also, vehicular emissions of oxidised nitrogen species such as NO_2 and HONO can be enhanced under 'cold-start'/cold driving conditions below 5 °C, a phenomenon that occurs for all fuel-types.[34] Further investigation of the source(s) of the 'primary' or 'direct' NO_2 emissions in Fairbanks is warranted in the context of the recently strengthened WHO air-quality guidelines[35] for NO_2 and to understand the impact of sources of oxidised reactive nitrogen on Fairbanks' wintertime atmospheric chemistry.

Conclusions

This study demonstrates low-cost electrochemical sensing of CO, NO, NO_2 and O_3 under cold and wide-ranging temperatures (0 °C down to −30 °C). We show that low-cost electrochemical gas sensors can deliver quantitative characterisation of atmospheric composition at the ppbv-level, which is sufficiently robust to investigate atmospheric chemistry. We demonstrate that autonomous instruments containing low-cost electrochemical sensors can provide continuous quantitative monitoring of Arctic atmospheric composition over week-to-month timescales, even under harsh Arctic conditions. Sensor deployments in downtown Fairbanks in February–March 2021 quantify $CO : NO_x$ compositions of local emissions and provide evidence for primary emissions of NO_2 that could be an important O_x oxidant source under the low ozone conditions of downtown Fairbanks in winter. Sensor deployments at two heights characterise the vertical distribution in air composition. Surface trapping of locally emitted pollutants at night occurs over very short vertical scales, which can be less than 20 m during strong temperature inversions. This leads to short-scale vertical gradients in oxidants relevant to atmospheric chemistry: surface ozone is depleted by NO_x

whilst ozone can be present at 20 m aloft. The inversions observed during February–March 2021 are short-lived as they are disrupted by efficient vertical mixing during the daytime due to solar heating. During the predominantly dark mid-winter, inversions and pollutant trapping can be longer-lived, leading to multi-day episodes of severe air quality. Local mediation efforts seek to further mitigate against poor air quality through reducing local emissions, building on achieved improvements in, *e.g.*, CO exceedances compared to previous decades.[4–6] However, the accumulation of pollutants at the surface is difficult to prevent when vertical mixing is limited by the development of stable temperature gradients in the Fairbanks basin, which is shielded by surrounding hills. The observed very short vertical scale of pollutant trapping with cleaner air just a few tens of meters aloft might offer potential for future geoengineering solutions to contribute to improving Fairbanks' indoor or outdoor air quality during severe surface pollution events, for example *via* introducing mechanical vertical mixing or using smart buildings with routing of clean air streams down from aloft, supported by automated real-time monitoring. This study presents low-cost electrochemical gas sensors as a valuable tool to measure atmospheric composition in the polluted Arctic at the ppbv-level, suitable for emission characterisation and for tracing atmospheric chemistry and fine-scale differences with height. The methods can also be applicable to the study of other urban wintertime environments where local emissions, temperature inversions and limited vertical mixing can lead to accumulation of pollutants at the surface and degraded air quality.

Data availability

Data for this article, including air-quality monitor and sensor gas measurements and mast-based temperature measurements, are available at OSF at **https://doi.org/10.17605/OSF.IO/UMDGW**.

Author contributions

All authors (T. J. Roberts, M. Cesler-Maloney, W. R. Simpson): conceptualization, methodology, software, validation, formal analysis, investigation, resources, data curation, writing – original draft, writing – review & editing, visualization, project administration, funding acquisition.

Conflicts of interest

There are no conflicts to declare.

Acknowledgements

This research analysis was undertaken through the ENS-PSLUniversity Actions Incitatives sENSe project and ANR consortium project VOLC-HAL-CLIM (ANR-18-CE01-0018), with small grant co-funding from Observatoire de Versailles Saint-Quentin-en Yvelines (OVSQ). It contributes essential sensor preparations for mobile vertical profiling applications planned in ANR CASPA, and for rooftop monitoring undertaken in ALPACA 2022. W. R. S. and M. C.-M. acknowledge

support from NSF grant NNA-1927750. We thank University of Alaska Fairbanks, the UAF Community and Technical College, and the Geophysical Institute for logistical support.

References

1 J. Schmale, S. R. Arnold, K. S. Law, T. Thorp, S. Anenberg, W. R. Simpson and A. Pratt, *Earth's Future*, 2018, **6**(10), 1385–1412, DOI: **10.1029/2018ef000952**.
2 T. Ward, B. Trost, J. Conner, J. Flanagan and R. K. M. Jayanty, *Aerosol Air Qual. Res.*, 2012, **12**(4), 536–543, DOI: **10.4209/aaqr.2011.11.0208**.
3 Y. Wang and P. K. Hopke, *Aerosol Air Qual. Res.*, 2014, **14**(7), 1875–1882, DOI: **10.4209/aaqr.2014.03.0047**.
4 J. Holty, *Arctic*, 1973, **26**(4), 292–302.
5 T. M. Gilmore and T. R. Hanna, *J. Air Pollut. Control Assoc.*, 1974, **24**(11), 1077–1079.
6 S. A. Bowling, *J. Clim. Appl. Meteorol.*, 1986, **25**, 22–34.
7 H. N. Q. Tran and N. Mölders, *Atmos. Res.*, 2011, **99**(1), 39–49, DOI: **10.1016/j.atmosres.2010.08.028**.
8 C. D. Whiteman, S. W. Hoch, J. D. Horel and A. Charland, *Atmos. Environ.*, 2014, **94**, 742–753, DOI: **10.1016/j.atmosenv.2014.06.012**.
9 Y. Largeron and S. Staquet, *Atmos. Environ.*, 2016, **135**, 92–108, DOI: **10.1016/j.atmosenv.2016.03.045**.
10 A. G. Hallar, S. S. Brown, E. Crosman, *et al.*, *Bull. Am. Meteorol. Soc.*, 2021, **102**(10), E2012–E2033, DOI: **10.1175/BAMS-D-20-0017.1**.
11 S. M. Bourne, U. S. Bhatt, J. Zhang J and R. Thoman, *Atmos. Res.*, 2010, **95**(2–3), 353–366, DOI: **10.1016/j.atmosres.2009.09.013**.
12 J. A. Mayfield and G. J. Fochesatto, *J. Appl. Meteorol. Climatol.*, 2013, **52**(4), 953–973, DOI: **10.1175/jamc-d-12-01.1**.
13 M. Cesler-Maloney, W. R. Simpson, T. Miles, J. Mao, K. S. Law and T. J. Roberts, *J. Geophys. Res.:Atmos.*, 2022, **127**, e2021JD036215, DOI: **10.1029/2021JD036215**.
14 E. S. Robinson, M. Cesler-Maloney, X. Tan, J. Mao, W. R. Simpson and P. F. Decarlo, *Environ. Sci.: Atmos.*, 2023, **3**, 568–580, DOI: **10.1039/d2ea00140c**.
15 M. I. Mead, O. A. M. Popoola, G. B. Stewart, P. Landshoff, M. Calleja, M. Hayes, J. J. Baldovi, M. W. McLeod, T. F. Hodgson, J. Dicks, A. Lewis, J. Cohen, R. Baron, J. R. Saffell and R. L. Jones, *Atmos. Environ.*, 2013, **70**, 186–203.
16 I. Heimann, V. B. Bright, M. C. McLoed, M. I. Mead, O. A. M. Popoola, G. B. Stewart and R. L. Jones, *Atmos. Environ.*, 2015, **113**, 10–19, DOI: **10.1016/j.atmosenv.2015.04.057**.
17 W. Jiao, G. Hagler, R. Williams, R. Sharpe, R. Brown, D. Garver, R. Judge, M. Caudill, J. Rickard, M. Davis, L. Weinstock, S. Zimmer-Dauphinee and K. Buckley, *Atmos. Meas. Tech.*, 2016, **9**, 5281–5292, DOI: **10.5194/amt-9-5281-2016**.
18 A. C. Lewis, J. D. Lee, P. M. Edwards, M. D. Shaw, M. J. Evans, S. J. Moller, K. R. Smith, J. A. Buckley, M. Ellis, S. R. Gillot and A. White, *Faraday Discuss.*, 2016, **189**, 85–103.
19 N. Castell, F. R. Dauge, P. Schneider, M. Vogt, U. Lerner, B. Fishbain, D. Broday and A. Bartonova, *Environ. Int.*, 2017, **99**, 293–302, DOI: **10.1016/j.envint.2016.12.007**.

20 E. S. Cross, L. R. Williams, D. K. Lewis, G. R. Magoon, T. B. Onasch, M. L. Kaminsky, D. R. Worsnop and J. T. Jayne, *Atmos. Meas. Tech.*, 2017, **10**, 3575–3588, DOI: **10.5194/amt-10-3575-2017**.

21 X. Pang, M. D. Shaw, A. C. Lewis, L. J. Carpenter and T. Batchellier, *Sens. Actuators, B*, 2017, **240**, 829–837, DOI: **10.1016/j.snb.2016.09.020**.

22 N. Zimmerman, A. A. Presto, P. N. S. Kuma, J. Gu, A. Haruyliuk, E. S. Robinson, A. L. Robinson and R. Subramanian, *Atmos. Meas. Tech.*, 2018, **11**, 291–313, DOI: **10.5194/amt-11-291-2018**.

23 R. Baron and J. Saffell, *ACS Sens.*, 2017, **2**(11), 1553–1566, DOI: **10.1021/acssensors.7b00620**.

24 D. E. William, *ACS Sens.*, 2019, **4**, 2558–2565, DOI: **10.1021/acssensors.9b01455**.

25 B. Crawford, D. H. Hagan, I. Grossman, E. Cole, L. Holland, C. L. Heald and J. H. Kroll, *Proc. Natl. Acad. Sci. U.S.A.*, 2021, **118**(27), e2025540118, DOI: **10.1073/pnas.2025540118**.

26 T. Bush, N. Papaioannou, F. Leach, F. D. Pope, A. Singh, G. N. Thomas, B. Stacey and S. Bartington S, *Atmos. Meas. Tech.*, 2022, **15**, 3261–3278, DOI: **10.5194/amt-15-3261-2022**.

27 R. Whitty, M. Pfeffer, E. Ilyinskaya, T. Roberts, A. Schmidt, S. Barsotti, W. Strauch, L. Crilley, F. Pope, H. Bellanger, E. Mendoza, T. Mather, E. Liu, N. Peters, I. Taylor, H. Francis, X. Hernández Leiva, D. Lynch, S. Nobert and P. Baxter, *Volcanica*, 2022, **5**(1), 33–59, DOI: **10.30909/vol.05.01.3359**.

28 T. J. Roberts, C. F. Braban, C. Oppenheiler, R. S. Martin, R. A. Freshwater, D. H. Dawson, P. T. Griffiths, R. A. Cox, J. R. Saffell and R. L. Jones, *Chem. Geol.*, 2012, **332–333**, 74–91, DOI: **10.1016/j.chemgeo.2012.08.027**.

29 M. Hossain, J. R. Saffell and R. Baron R, *ACS Sens.*, 2016, **1**(11), 1291–1294, DOI: **10.1021/acssensors.6b00603**.

30 TUV model website, **https://www2.acom.ucar.edu/modeling/tropospheric-ultraviolet-and-visible-tuv-radiation-model**, **https://www.acom.ucar.edu/Models/TUV/Interactive_TUV/**.

31 N. Brett, K. S. Law, S. R. Arnold *et al.*, *ACPD preprint in review*, 2022, DOI: **10.5194/egusphere-2024-1450**.

32 S. K. Grange, A. C. Lewis, S. J. Moller and D. C. Carslaw, *Nat. Geosci.*, 2017, **10**, 914–918, DOI: **10.1038/s41561-017-0009-0**.

33 R. J. Wild, W. P. Dubae, K. Aikin, S. J. Eilerman, A. Neuman, J. Peischl, T. B. Ryerson and S. S. Brown, *Atmos. Environ.*, 2017, **148**, 182–189, DOI: **10.1016/j.atmosenv.2016.10.039**.

34 V. N. Matthaios, L. J. Kramer, R. Sommariva, F. D. Pope and W. J. Bloss, *Atmos. Environ.*, 2019, **199**, 402–414, DOI: **10.1016/j.atmosenv.2018.11.031**.

35 World Health Organization, *WHO Global Air Quality Guidelines*, 2021, **https://apps.who.int/iris/handle/10665/345334**, Licence: CC BY-NC-SA 3.0 IGO.